

Article

Synthesis of Complex Concentrated Nanoparticles by Ultrasonic Spray Pyrolysis and Lyophilisation

Lidija Simić ¹, Srečko Stopic ², Bernd Friedrich ², Matej Zadavec ¹, Žiga Jelen ¹, Rajko Bobovnik ³, Ivan Anžel ¹ and Rebeka Rudolf ^{1,4,*}

¹ Faculty of Mechanical Engineering, University of Maribor, Smetanova ulica 17, 2000 Maribor, Slovenia

² IME Process Metallurgy and Metal Recycling, RWTH Aachen University, Intzestrasse 3, 52056 Aachen, Germany

³ Faculty of Polymer Technology, Ozare 19, 2380 Slovenj Gradec, Slovenia

⁴ Zlatarna Celje d. o. o., Kersnikova 19, 3000 Celje, Slovenia

* Correspondence: rebeka.rudolf@um.si; Tel.: +386-41735-300

Abstract: The development of new multicomponent nanoparticles is gaining increasing importance due to their specific functional properties, i.e., synthesised new complex concentrated nanoparticles (CCNPs) in the form of powder using ultrasonic spray pyrolysis (USP) and lyophilisation from the initial cast Ag₂₀Pd₂₀Pt₂₀Cu₂₀Ni₂₀ alloy, which was in the function of the material after its catalytic abilities had been exhausted. Hydrometallurgical treatment was used to dissolve the cast alloy, from which the USP precursor was prepared. As a consequence of the incomplete dissolution of the cast alloy and the formation of Pt and Ni complexes, it was found that the complete recycling of the alloy is not possible. A microstructural examination of the synthesised CCNPs showed that round and mostly spherical (not 100%) nanoparticles were formed, with an average diameter of 200 nm. Research has shown that CCNPs belong to the group with medium entropy characteristics. A mechanism for the formation of CCNPs is proposed, based on the thermochemical analysis of element reduction with the help of H₂ and based on the mixing enthalpy of binary systems.

Keywords: complex concentrated nanoparticles; ultrasonic spray pyrolysis; lyophilisation; characterisation; formation mechanism



Citation: Simić, L.; Stopic, S.; Friedrich, B.; Zadavec, M.; Jelen, Ž.; Bobovnik, R.; Anžel, I.; Rudolf, R. Synthesis of Complex Concentrated Nanoparticles by Ultrasonic Spray Pyrolysis and Lyophilisation. *Metals* **2022**, *12*, 1802. <https://doi.org/10.3390/met12111802>

Academic Editor: Petros E. Tsakiridis

Received: 1 September 2022

Accepted: 20 October 2022

Published: 24 October 2022

Publisher's Note: MDPI stays neutral with regard to jurisdictional claims in published maps and institutional affiliations.



Copyright: © 2022 by the authors. Licensee MDPI, Basel, Switzerland. This article is an open access article distributed under the terms and conditions of the Creative Commons Attribution (CC BY) license (<https://creativecommons.org/licenses/by/4.0/>).

1. Introduction

The demand for materials with high performance as well as functional properties is the driving force for the research of new, complex alloys, as well as their machining processes [1]. The development of complex concentrated alloys (CCAs) enables the design of new classes of materials with a new/better combination of properties, due to a larger number of main elements [2,3]. The chemical composition of this group of alloys covers the central regions in phase diagrams. As a result, researchers today face a great challenge, which is the discovery of an incredibly large number of new alloys that still belong to unexplored parts of multicomponent phase diagrams.

The development of nanotechnology is becoming increasingly important in various research fields due to the need for different nanomaterials in terms of their shapes, sizes, and chemical composition. This dictates the use of improvised techniques, as well as controlled spraying, which may enable the extraction of nanoparticles [4]. Special attention to nanostructured materials is necessary in multicomponent metal nanostructures. One such group of nanostructure sources is from CCAs, in which the maximum interactions of different metal atoms lead to the formation of a unique structure with a high configurational entropy of mixing [5]. CCAs can be classified as high-entropy alloys (HEAs), if the achieved configurational entropy is greater than or equal to 1.5 R [6]. Due to the specific combination of mechanical and functional properties, these alloys are attracting increasing interest [3].

The most commonly used methods for CCA–nanoparticle synthesis are mechanical alloying, wet chemistry methods, laser coating, and thermal spraying, which allows for the easy preparation of nanocrystalline or amorphous particles with uniform structures and distribution of components. The formation of metal nanostructures by traditional wet chemistry procedures is difficult due to different chemical reactions in one precursor system and a very short retention time [5].

One of the potential methods is the production of nanoparticles by ultrasonic spray pyrolysis (USP), which is a very fast, continuous, and relatively flexible technique [7,8]. The first step in USP synthesis is the formation of an aerosol generated by ultrasound from a precursor that contains metal ions in drops of solute (usually water). The choice of the appropriate precursor as well as the solute concentration are very important factors because the chemical composition of the desired nanoparticles depends on them, as well as on the technological transport by carrier gas into the evaporation zone, where water evaporation takes place. In the next stage, dry droplets enter into the reaction zone, where chemical decomposition takes place at high temperatures in the presence of reaction gas [7]. The influence of different USP parameters, such as solution concentrations, ultrasonic frequencies, temperature, as well as the synthesis mechanisms of metal, oxide, composite nano-quantities, and submicron particles are mainly described in the studies of Stopić et al. [9,10]. Additionally, an important advantage of the USP method can be found in the recycling by synthesis of nanoparticles from the initial scrap [11]. As material recycling becomes more and more important regardless of numerous obstacles [12], by synthesising nanoparticles from the initial cast $\text{Ag}_{20}\text{Pd}_{20}\text{Pt}_{20}\text{Cu}_{20}\text{Ni}_{20}$ alloy (which will be used for catalytic purposes), we will try to prove that it is possible to reuse the catalytically used material ($\text{Ag}_{20}\text{Pd}_{20}\text{Pt}_{20}\text{Cu}_{20}\text{Ni}_{20}$) by recycling it through the synthesis of the nanoparticles. Due to complicated chemical reactions in one system and the very short retention time, the synthesis of nanoparticles such as CCNPs presents a major challenge when using one-step USP. The chemical composition of the alloy was chosen under the assumption that this alloy had a high catalytic potential [13–16], as well as a high configurational entropy of mixing ($\Delta S_{\text{mik}}^{\text{conf}} = 1.61 \text{ R}$) [17].

Previous research in the field of synthesis of multi-component noble nanoparticles represents the successful synthesis of bimetallic [18,19] and trimetallic nanoparticles from the initial aqueous solution. AgPd and AgPt are used to improve catalysis in H_2O_2 generation, while Cu-based particles such as CuPt and AgCuPt have been observed to exhibit high catalytic activity in the electrochemical reduction in CO_2 [19].

Based on our knowledge, references [4,20,21], and potential recycling, we tried to synthesise CCNPs from the cast alloy with an identical chemical composition using the USP. A hydrometallurgical approach was used to prepare the precursor by dissolving the initial cast $\text{Ag}_{20}\text{Pd}_{20}\text{Pt}_{20}\text{Cu}_{20}\text{Ni}_{20}$ alloy with various acids. Synthesised CCNPs by USP are collected in suspension, and in order to obtain the CCNP powder it was necessary to remove the suspension by drying process. Freeze-drying is offered as one of the options (as lyophilisation), wherein it is possible to obtain nanoparticles in powder form, and thus achieve their use for further applications [22–24]. The mechanism for the formation of CCNPs was established at the end of the research.

The aim of this study was to show that existing catalytic materials with a similar chemical composition can be reused in the post-use phase—when they become so-called waste—based on two new methods: USP synthesis and lyophilisation. The requirement was to achieve a new material similar to dried nanoparticles, with completely different, but useful, “functional” properties, for new and still unknown applications. In this way, the possibility of synthesising nanoparticles from an alloy that no longer has catalytic properties was demonstrated.

2. Materials and Methods

The proposed methodology, which consists of a few stages, is presented in Figure 1.

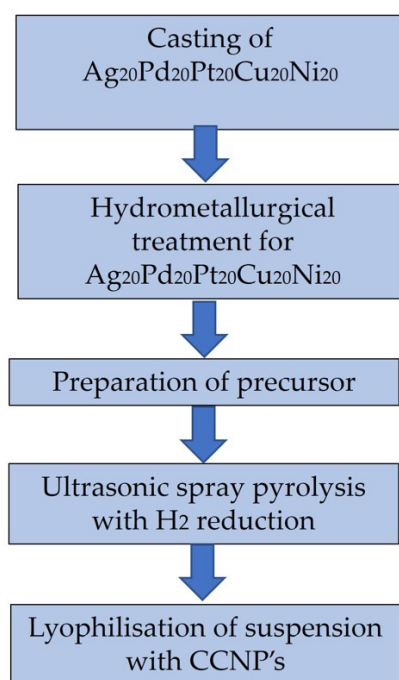


Figure 1. Proposed methodology of procedures for the synthesis of CCNPs.

2.1. Casting of $Ag_{20}Pt_{20}Pd_{20}Cu_{20}Ni_{20}$

The alloy was prepared in an induction furnace Aurodent (Zlatarna Celje, Celje, Slovenia) in a protective atmosphere of Ar 5.0, by melting the pure components (Ag granules—99.99 wt. %; Pd sponges—99.99 wt. %; Pt sponges—99.99 wt. %; Cu granules—99.9 wt. %; Ni tiles—99.99 wt. %). No oxidation was detected. Melting was performed at 1400 °C for 15 min. The liquid melt was cast in a heated iron mould. Determination of the degree of metastability of this cast $Ag_{20}Pt_{20}Pd_{20}Cu_{20}Ni_{20}$ alloy was presented in a previous work [17].

2.2. Hydrometallurgical Treatment

Dissolution of the cast $Ag_{20}Pt_{20}Pd_{20}Cu_{20}Ni_{20}$ alloy was performed in specially designed equipment in an ultrasonic bath in SONOREX, Bandeline, Germany. The analysis of hydrometallurgical treatment of alloys with nitric acid contains chemical reactions related to the dissolution of silver, platinum, palladium, copper, and nickel.

Based on the analysis of the chemical reactions, nitric acid was chosen as a leaching agent forming palladium nitrate, platinum nitrate, silver nitrate, nickel nitrate, and copper nitrate.

Dissolution of the material was performed in 65% nitric acid (Merck, Darmstadt, Germany) in an ultrasonic bath at room temperature, which was used for faster dissolution. To improve the dissolution of the alloy, the used concentration of nitric acid was 9.16 mol/l, and the temperature was increased to 60 °C. Additional air introduction was used to increase the oxidation of the alloy. Ultrasonic rinsing allows for better mixing in the system and dissolution. The use of nitric acid does not allow for the complete dissolution of the starting cast alloy. After dissolution, precipitates were formed, which were removed from the solution.

2.3. Thermochemical Analysis of Hydrogen Reduction

Using the HSC software package 6.12 (Outotec, Espoo, Finland), Figure 2 shows the thermochemical analysis of the hydrogen reduction in metals (Ag, Pd, Cu, and Ni), which in all cases have a negative Gibbs energy value at 700 °C. From Figure 2, it is also possible to see the high probability of the formation of metal nanoparticles under these conditions. The

results of the thermochemical analysis of Pt are not shown, because the existing data were not found in the HSC program. Additionally, taking into account the fact that bimetallic Ni-Pt nanoparticles can be used for H₂ storage [24], it can be assumed that Ni and Pt will not react to the same extent as other elements with H₂.

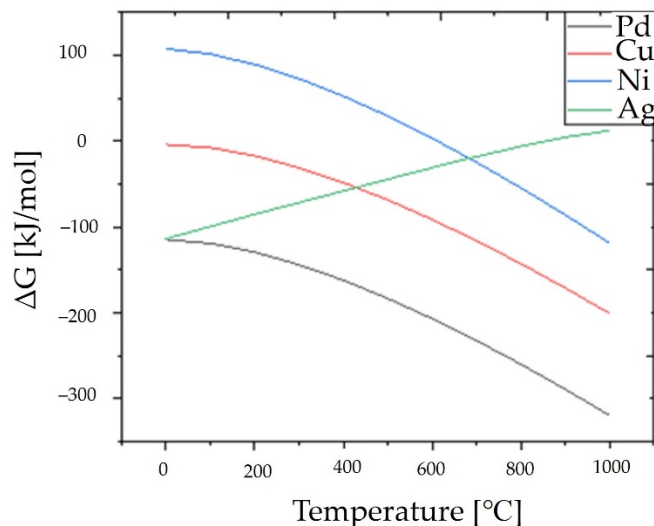


Figure 2. Thermochemical analysis of hydrogen reduction in Pd, Cu, Ni, and Ag.

The use of solution thermochemistry was not considered in this study due to two important limitations of the HSC software. At different pH values and potential Eh of the aqueous solution, its thermochemistry can be analysed for a maximum of three metals and only one acidic ion at the same time (Eh–pH diagrams), but not for five elements and two acidic ions, which are present in our dissolution of the high-entropy alloy.

2.4. USP Synthesis

The synthesis of the CCNPs was performed by single-stage USP as shown in Figure 3.

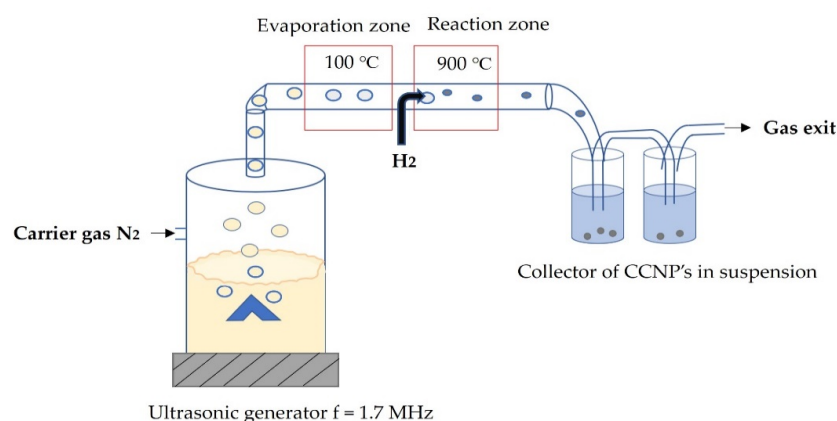


Figure 3. Schematic representation of CCNPs' synthesis via USP.

Very fine aerosol droplets ($2r < 5 \mu\text{m}$) of the prepared precursor were obtained with an ultrasonic nebuliser (PRIZMNano, Kragujevac, Serbia) with a frequency of 1.7 MHz in an ultrasonic field obtained using 3 ultrasonic transducers. The aerosol was transported with a flow of nitrogen of 1.0 and hydrogen of 1.0 L/min in a quartz tube (145 cm long and 5 cm in diameter) in the laboratory tubular furnace (Ströhlein, Selm, Germany). Temperature in the reaction zone was 900 °C.

Synthesised CCNPs were collected in two bottles with a suspension of water and PVP with the concentration of 12.5 g/L PVP (K30, Thermo Fisher Scientific Inc., Schwerte, Ger-

many). PVP was added to provide stability and prevent agglomeration of the synthesised CCNPs [7,25–27].

2.5. Lyophilisation

For the CCNPs to be used for further analysis, the suspension containing the CCNPs must be dried. Freeze-drying (lyophilisation) of the suspension was performed instead of classical convection drying, to avoid the movement of the liquid during drying and agglomeration of the particles [28,29]. The freeze-drying process itself is limited to the removal of water from the product while the product remains intact, which is why it is most commonly used in the pharmaceutical industry [30,31]. To ensure a successful process, drying was carried out in several steps. The first step of drying is freezing the water at low temperatures, after which the pressure drops. The second step is the direct sublimation of the frozen water (water crystal) with the necessary heat, i.e., the transition from the solid to the gaseous state [21]. The drying process must be carried out under optimal conditions to avoid sedimentation, agglomeration, and other side effects. The process conditions, such as primary drying temperature and pressure and secondary drying temperature and pressure, were selected following previous drying cycles for different formulations of nanoparticles [21,29]. These conditions prevented sedimentation, agglomeration (SEM analysis), and collapse of the dried material (the dried material cake was stable and did not collapse).

A freeze dryer, LIO-2000 FLT (Kambič DOO, Semič, Slovenia), was used for freeze-drying [32]. The freeze-drying protocol (see Figure 4) was measured with four thermocouples (T_{shelf} —shelf temperature, T_1 —temperature at the bottom of the sample, T_2 —temperature in the middle of the sample, and T_3 —temperature at the top of the sample). The thermocouple T_2 was placed at a height of 0.63 cm from T_1 , while T_3 was placed at a height of 0.63 cm from T_2 , as seen in Figure 4a.

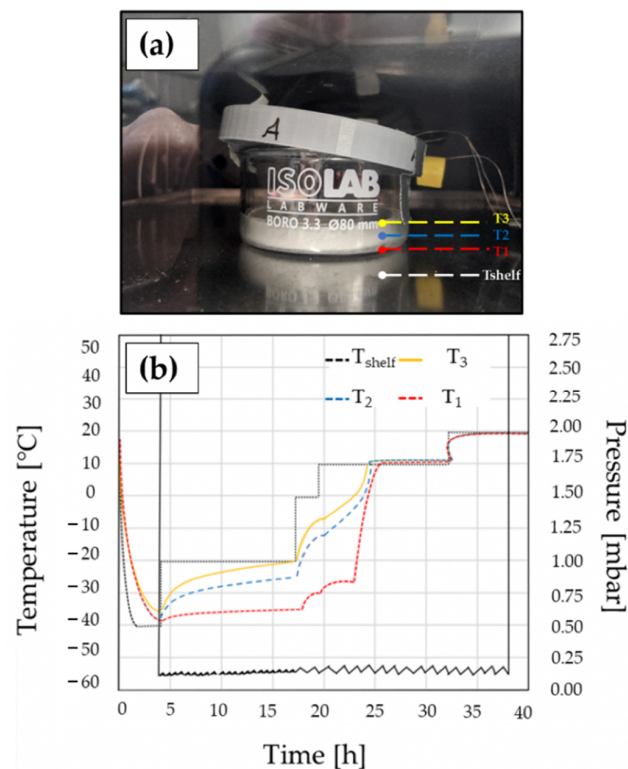


Figure 4. (a) Drying sample on a lyophiliser shelf with thermocouples (T_{shelf} —shelf temperature, T_1 —temperature of the bottom of the sample, T_2 —temperature of the middle of the sample, and T_3 —temperature of the top of the sample); (b) Lyophilisation drying protocol (shelf temperatures and vacuum level) with monitored temperatures.

From Figure 4b, it can be seen that the freezing phase occurred at a shelf temperature of $-40\text{ }^{\circ}\text{C}$ during the first 3.5 h of the process. The first drying phase took place at $-20\text{ }^{\circ}\text{C}$ for about 13 h, followed by the second phase at $0\text{ }^{\circ}\text{C}$. After a total of 19 h, the temperature was increased to $10\text{ }^{\circ}\text{C}$. Thereafter, the temperature was increased to $20\text{ }^{\circ}\text{C}$ to determine the completion of the drying process. By combining the fast and slow freezing shown in Figure 4, we avoided agglomeration and sedimentation.

3. Characterisation

3.1. XRF—X-ray Fluorescence Spectroscopy of the Cast $\text{Ag}_{20}\text{Pd}_{20}\text{Pt}_{20}\text{Cu}_{20}\text{Ni}_{20}$ Alloy

The wt. % of all elements in the cast $\text{Ag}_{20}\text{Pd}_{20}\text{Pt}_{20}\text{Cu}_{20}\text{Ni}_{20}$ alloy was measured by XRF (Niton XL3t GOLDD+, Thermo Scientific, Munich, Germany). A piece of cast sample $3\text{ mm} \times 3\text{ mm} \times 3\text{ mm}$ in size was used for measurement.

3.2. ICP—OES—Inductively Coupled Plasma—Optical Emission Spectrometry

3.2.1. Precursor

The concentrations of all elements in the precursor solution were measured by ICP—OES (SPECTRO ARCOS, SPECTRO Analytical Instruments GmbH, Kleve, Germany). Nitric acid (HNO_3 , Merck, Darmstadt, Germany), AppliChem, 65% concentrated, was used to treat the solution. The sample was only diluted from 0.5 mL to 50 mL. The sample intake was 0.8 mL/min. The relative measurement uncertainty was estimated at $\pm 3\%$.

3.2.2. Suspension with CCNPs

The concentrations of all five elements (Ag, Pd, Pt, Cu, and Ni) in the CCNPs dispersed in suspension were measured by the same ICP—OES (SPECTRO ARCOS, SPECTRO Analytical Instruments GmbH, Kleve, Germany) device and under the same parameters as by the precursor measurements (see Section 3.2). A total of 5 mL of suspension was used for the measurement.

3.3. DLS Method and Zeta Potential Measurements

DLS measurement was used to measure the hydrodynamic size distribution of the spherical CCNPs in the suspension. Measuring the zeta potential or electric charge determined an important indicator of the suspension's stability.

The measurements were performed using a Malvern Zeta sizer Nano ZS instrument (Malvern Panalytical, Worcestershire, UK) with a disposable plastic cuvette. The measurement of the zeta potential was performed using a closed capillary cell with electrodes, at a temperature of $25\text{ }^{\circ}\text{C}$. The dispersant of the suspension is deionised water, viscosity, absorption, and other factors which are unknown, because it is an unknown material.

3.4. XRD Analysis of Formed Precipitate

XRD analysis was used to detect the crystallographic phases of the precipitate formed during the dissolution of the cast alloy. X-ray powder diffraction—a Panalytical X'pert Pro PW 3040/60 goniometer (Malvern Products, Malvern, UK)—was used to measure 2θ between 0° and 95° with a step size of 0.002° and a scan step time of 50 s on each recorded step with Bragg—Brentano optics. The Cu anode with $K\alpha = 0.154\text{ nm}$ was used with a current of 40 mA and a potential of 45 kV.

3.5. SEM Observations with EDS Analysis

SEM (JEOL-6380 LV, Tokyo, Japan) was used to characterise the shape, size, and morphology of the lyophilised CCNPs, while an EDS detector (JSM-6000, JEOL, Tokyo, Japan) was used for semiquantitative and semiquantitative microchemical analysis. The sample was prepared for SEM analysis by sticking a piece of lyophilised CCNPs to a copper tape and then crushing it. Point analyses were performed under initial parameters: high vacuum (HV) at 15–30 kV, with magnifications between 25,000 and $100,000\times$. Based on

the obtained SEM micrographs, it was possible to perform an analysis of the shape and morphology of the CCNPs.

3.6. TEM

JEOL 2100 (JEOL, Japan) and JEOL JEM-2200FS HR (JEOL, Japan) equipment operating at 200 kV were used for the TEM observations. A drop of suspension with CCNPs was placed on a copper TEM mesh with an amorphous carbon film. The holder was then dried before being used for the TEM research.

3.7. Statistics

ImageJ software (ImageJ 1.x, National Institute of Mental Health, Washington, DC, USA) was used to measure the CCNPs with SEM micrographs. A total of 200 CCNPs were measured from the SEM images. The mean values of the standard deviation from the measured particle sizes were calculated for each sample according to the standard [33].

4. Results and Discussion

4.1. XRF of Cast Alloy

Table 1 shows the wt. % of each element in the cast $\text{Ag}_{20}\text{Pd}_{20}\text{Pt}_{20}\text{Cu}_{20}\text{Ni}_{20}$ alloy measured by XRF analysis and expressed additionally in at. %. The loss of 1 at. % was remarked for Ag and Pd, while the contents of Pt and Cu were almost adequate, or, in the case of Ni, the content was higher by more than 1 at. %.

Table 1. XRF analysis of cast $\text{Ag}_{20}\text{Pd}_{20}\text{Pt}_{20}\text{Cu}_{20}\text{Ni}_{20}$ alloy.

Element	Ag	Pd	Pt	Cu	Ni
wt. %	0.0062	0.010	0.0092	0.0074	0.0016
at. %	18.83	19.40	20.46	20.10	21.21

4.2. ICP-OES

4.2.1. Precursor

Table 2 showed the ICP–OES results in g/L values for the elements Ag, Pd, Pt, Cu, and Ni, and the additional calculation of the obtained values was performed in at. %, as seen in Table 2.

Table 2. ICP–OES analysis of the precursor.

Element	Ag	Pd	Pt	Cu	Ni
g/L	0.64	0.85	0.58	0.51	0.06
at. %	22.87	30.79	11.47	30.94	3.93

From the initial sample of the cast $\text{Ag}_{20}\text{Pd}_{20}\text{Pt}_{20}\text{Cu}_{20}\text{Ni}_{20}$ alloy was dissolved: 22.87 at. % Ag, 30.79 at. % Pd, 11.46 at. % Pt, 30.94 at. % Cu, and 3.93 at. % Ni. The incomplete dissolution of Pt can be attributed to the very slow dissolution reaction of Pt in concentrated HCl [34]. The very weak dissolution of Ni can be attributed to the positive mixing enthalpy of the Ag–Ni system, whereby the system tends to separate [35].

A solution with the chemical composition presented in Table 1 was used as a precursor for the synthesis of CCNPs using USP. In order to perform a comparison of the chemical composition of the cast alloy and the CCNPs, and therefore determine whether partial recycling is possible, the precursor correction was not performed in the chemical composition for USP.

4.2.2. Suspension with CCNPs

The ICP–OES analysis of the synthesised CCNPs in suspension showed the following values (g/L) for elements and calculated values in at. % in Table 3:

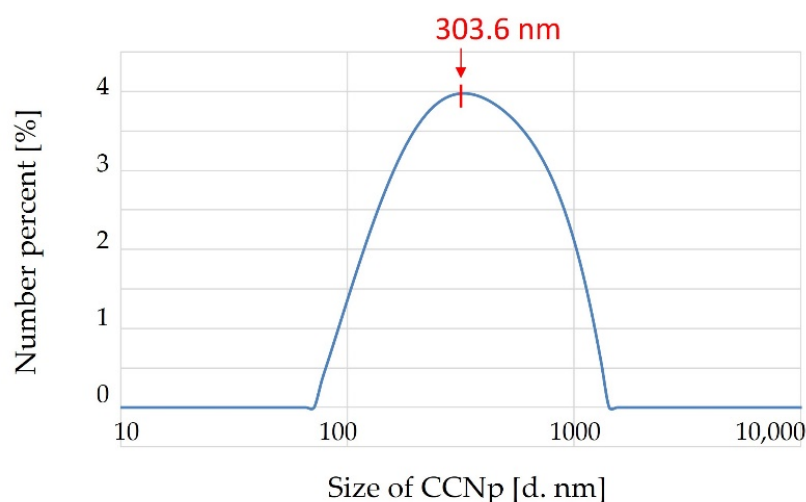
Table 3. ICP–OES analysis of suspension with CCNPs.

Element	Ag	Pd	Pt	Cu	Ni
g/L	6.2	10.2	9.2	7.4	1.6
at. %	16.62	27.73	13.60	34.24	7.81

The measured values indicate that the chemical composition of the synthesised CCNPs differs from the initial composition of the precursor, as seen in Table 2. The greatest chemical matches were observed for Pd, Pt, and Cu, while the concentrations of Ag and Ni differed significantly. The ratio of the precursors and CCNPs by individual elements was as follows: Ag:Pt:Cu:Ni—1.3:1.1:0.8:0.9:0.5.

4.3. DLS Method and Zeta Potential Measurements

The hydrodynamic diameter of the CCNPs ranged from approximately 80 nm to 1300 nm, with an average value of 303.6 ± 28.04 nm and with a size polydispersity index of 0.261, as shown in Figure 5.

**Figure 5.** Distribution of CCNPs using DLS analysis.

The zeta potential of the NPs' surface was -7.87 ± 0.59 mV. This value indicates that the CCNPs were not stable and had a high tendency to agglomerate, so a steric stabiliser such as PVP was used in the suspension.

4.4. XRD Results

The recorded XRD spectrum of the precipitate has more than 50 peaks in the range 2θ between 10° and 90° (Figure 6). Based on this, only the main peaks were considered, so the presence of the three most prominent salts ($(\text{NH}_4)_2\text{PtCl}_6$, $(\text{NH}_3)_6\text{NiPtCl}_6 \times 0.5\text{H}_2\text{O}$, $\text{Pt}_2(\text{NH}_3)_4\text{Cl}_4$) was revealed. All the salts are illustrated with characteristic peaks that have been compared with the literature data on structural factors [36]—see the supplementary file.

4.5. SEM Observations with EDS Analysis

The incomplete dissolution and the formation of the precipitates were observed during the dissolution and preparation of the precursor. Figure 7a shows the filtered and dried insoluble precipitate, while Figure 7b shows a micro-view of the resulting precipitate. In order to determine the chemical composition of this precipitate, an EDS micro-analysis was performed. The six characteristic places of the point analysis are shown in Figure 7b, while the EDS results are shown in the lower part of Figure 7 as a table. The precipitate was rich in Pt, Ni, and Cl.

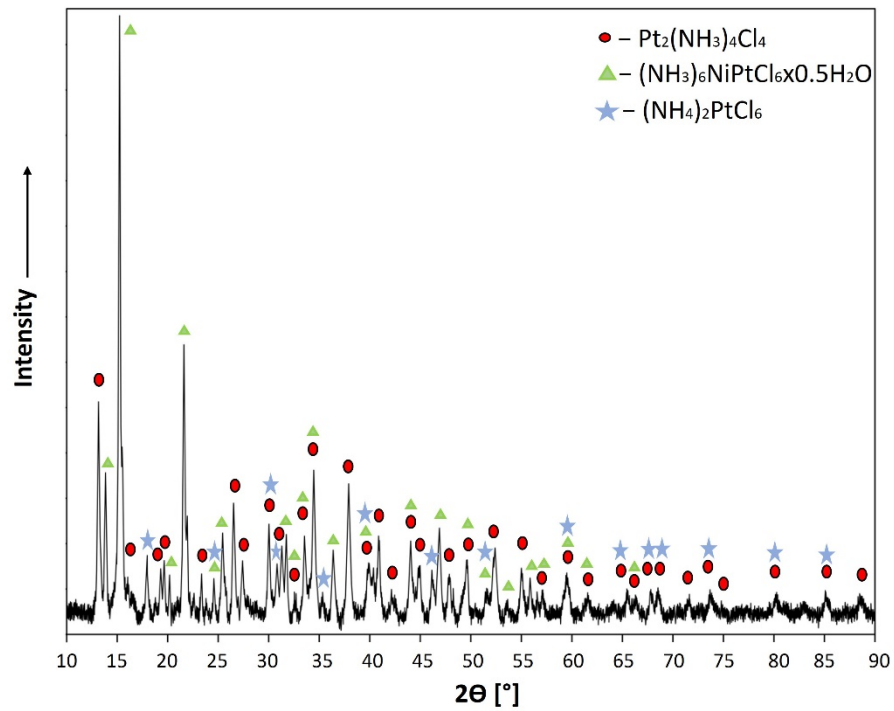
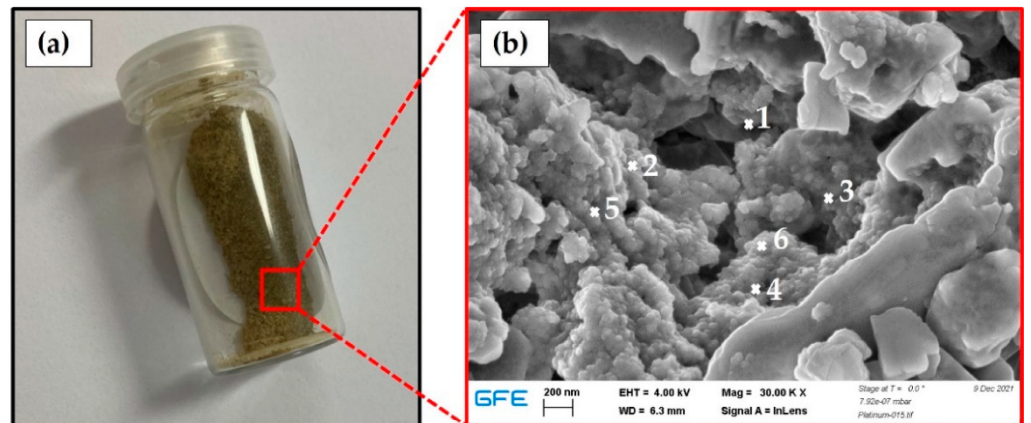


Figure 6. XRD analysis of the formed precipitate as residues by dissolving the cast alloy.

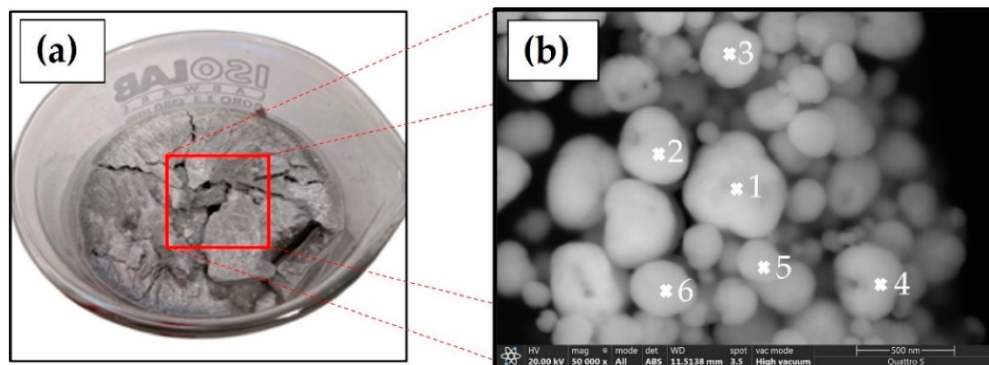


Spectrum	Pt	Cl	Ni
Spectrum 1	12.36	76.04	11.60
Spectrum 2	11.78	76.55	11.67
Spectrum 3	12.73	72.62	14.65
Spectrum 4	12.11	77.35	10.54
Spectrum 5	12.90	72.09	15.02
Spectrum 6	11.01	72.75	16.24
Mean	12.15	74.57	13.29
Std. Deviation	0.69	2.33	2.30
Max. value	12.90	77.35	16.24
Min. value	11.01	72.09	10.54

Figure 7. Insoluble precipitate: (a) Macro-view and (b) SEM microstructure showing places for EDS analysis.

SEM allowed for an observation of the shape, size, and morphology of the CCNPs. A microstructural examination revealed that CCNPs were round and mainly spherical (not 100%), with a diameter between 65 nm and 436 nm, as visible in Figure 8a. It can also be

seen clearly from Figure 8b that the lyophilisation parameters were optimal, because no sedimentation and agglomeration were observed. An EDS detector was used to identify the chemical composition. Figure 8b shows the typical places for the point analysis, while the results of the EDS analysis are presented immediately below in Figure 8.



Spectrum	Ag	Pd	Pt	Cu	Ni
Spectrum 1	21.87	34.37	14.13	24.97	4.66
Spectrum 2	21.64	35.31	12.02	26.18	4.86
Spectrum 3	19.89	34.18	13.45	28.13	4.36
Spectrum 4	22.86	35.08	12.25	25.19	4.63
Spectrum 5	22.81	36.00	12.86	24.27	4.05
Spectrum 6	19.91	35.45	12.70	27.89	4.06
Mean	21.50	35.06	12.90	26.10	4.44
Std. Deviation	1.33	0.69	0.78	1.60	0.33
Max. value	22.86	36.00	14.13	28.13	4.86
Min. value	19.89	34.18	12.02	24.27	4.05

Figure 8. CCNPs: (a) Macro-view and (b) SEM microstructure showing places for EDS analysis.

The different sizes of the CCNPs are a consequence of the droplets' coalescence during their transport through the furnace. DLS analysis measures the larger diameter, i.e., the hydrodynamic diameter, while the statistical data give a more realistic diameter [37]. According to the statistically calculated results, the approximate size of the synthesised CCNPs was 200 nm. According to the Standard ISO 1332-1:2004, the degree of roundness for CCNPs, if we take into account the 200 CCNPs from the SEM images, is 0.8486 ± 0.082035 (with a range of 0–1, 0—mark irregular shape; and 1—perfect circle). These values indicate that spherical-shaped CCNPs had been achieved practically.

The EDS analyses show the presence of all five elements in the CCNPs. The achieved chemical composition from EDS for CCNPs was approximately $\text{Ag}_{22}\text{Pd}_{35}\text{Pt}_{13}\text{Cu}_{26}\text{Ni}_4$ (in at. %). According to our calculated value for the configuration entropy of mixing, the CCNPs formed in this way belong to the group of medium entropy materials. Elemental mapping was conducted additionally, which showed the distribution of the elements on the CCNPs' surfaces. All five elements were distributed uniformly in the nanoparticles—as presented in Figure 9—suggesting that CCNPs were mixed atomically without phase separation.

Based on the EDS results and the thermochemical analysis of H_2 reduction for the elements Ag, Pd, Cu, and Ni (from Figure 2), it can be assumed that the mechanism of CCNPs' formation at 900 °C during USP synthesis occurred in the following sequence: $\text{Pd} > \text{Cu} > \text{Ag} > \text{Ni}$. This suggests that the elements do not segregate simultaneously and become embedded in the nanoparticle at once.

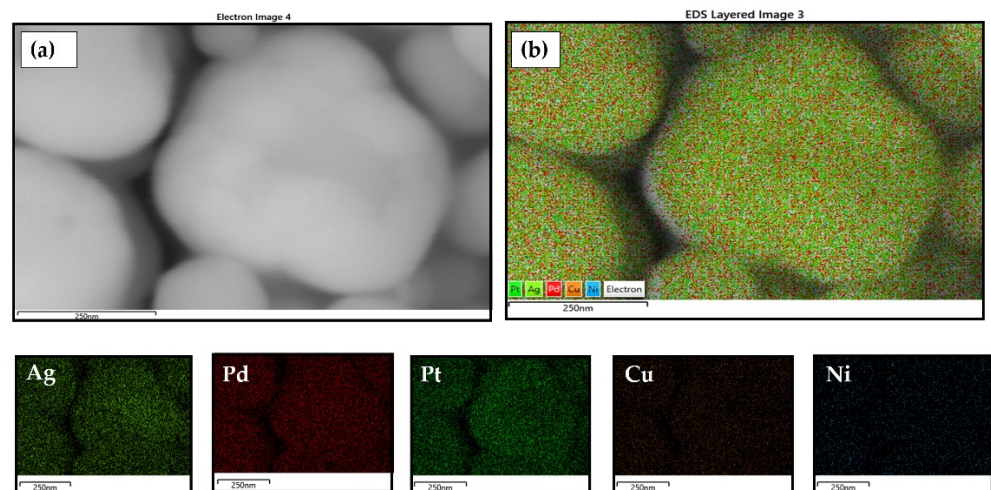


Figure 9. CCNPs: (a) SEM micrograph, (b) Elemental mapping of Ag, Pd, Pt, Cu, and Ni on the surface.

4.6. Transmission Electron Microscopy (TEM)

TEM analysis was used for a deeper observation of the CCNPs' morphology. The obtained results show an almost spherical shape (not 100%) of the CCNPs, as seen in Figure 10.

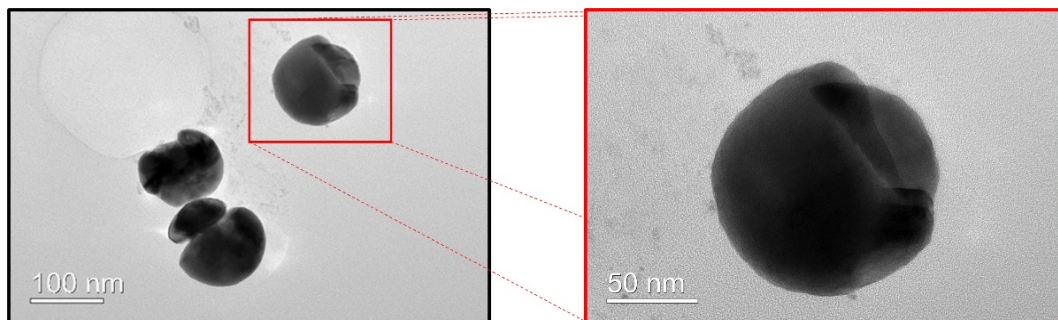


Figure 10. TEM view of CCNPs.

TEM revealed that CCNPs do not have a perfect spherical shape and are of different sizes. The result of the formation of such CCNPs can be the coagulation of droplets during their transportation to the furnace, as well as the inadequate conditions for the formation of CCNPs in the reaction zone.

The formation of CCNPs of different chemical compositions from the initial cast alloy can be attributed to a complex, incomplete dissolution. A schematic representation of the hydrometallurgical treatment of the cast alloy is shown in Figure 11, with a focus on changing the chemical composition by individual element.

It can be assumed that the main problem of the incomplete dissolution of Pt occurs due to the presence of Ag, which hinders the complete dissolution in HNO_3 [38]. In order to dissolve pure Pt in HCl, due to its high chemical stability, it takes a long time, as well as a considerable amount of acid with strong oxidants [34], which represents another possible factor for the incomplete dissolution of Pt. The dissolution of this alloy is a very complex problem, due to the five main elements that have different dissolution tendencies. In order to explain the incomplete dissolution of certain elements, as well as the mechanism of the CCNPs' formation, the approach used was the enthalpy of mixing of the binary system. This is presented in Table 4 [35]. In this way, the incomplete dissolution of Ni can be attributed to the high positive value of the enthalpy of mixing that it has with almost all the listed elements, as seen in Table 4, column 5.

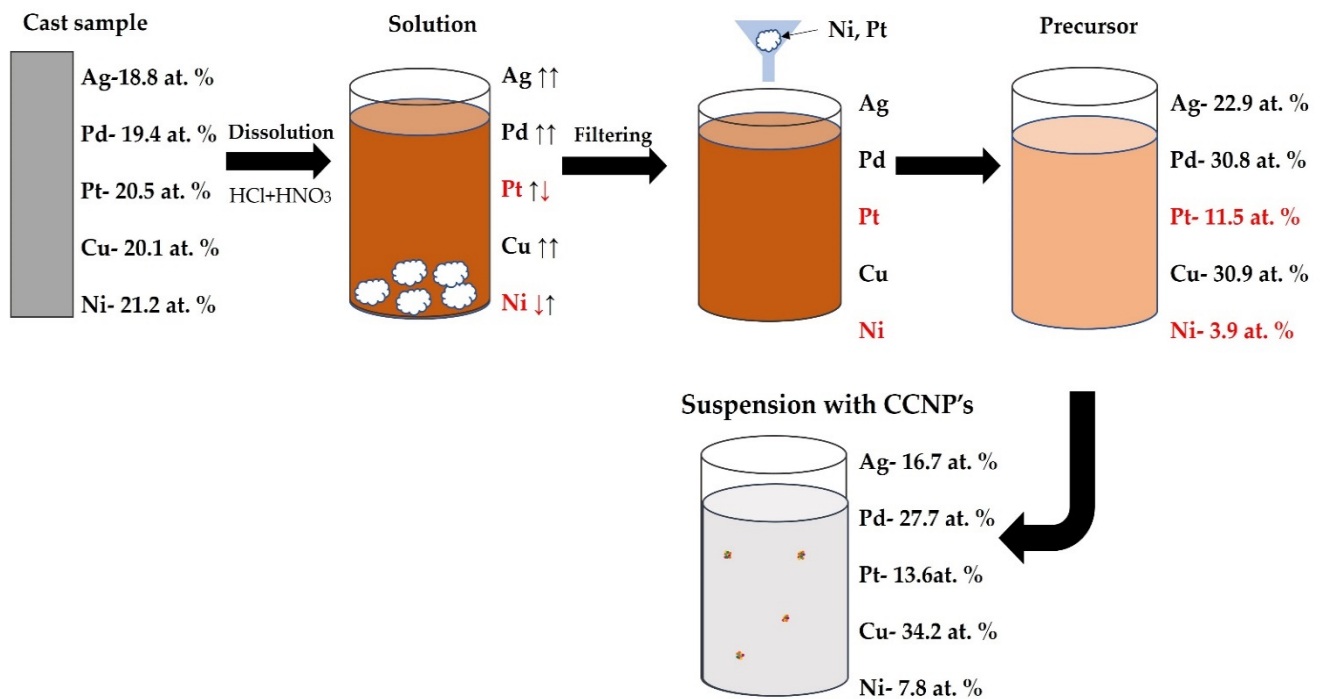


Figure 11. Schematic representation of the hydrometallurgical treatment of dissolution and precursor preparation.

Table 4. Mixing enthalpies of binary systems [35].

		ΔH_{mix} [kJ/mol]							
Ag		Pd		Pt		Cu		Ni	
AgPd	−7	PdAg	−7	PtAg	−1	CuAg	2	NiAg	15
AgPt	−1	PdPt	2	PtPd	2	CuPd	−14	NiPd	0
AgCu	2	PdCu	−14	PtCu	−12	CuPt	−12	NiPt	−5
AgNi	15	PdNi	0	PtNi	−5	CuNi	4	NiCu	4

As the dissolution of the cast alloy itself is complex, and, thus, the dissolution of the formed precursor, the enthalpies of mixing of individual binary systems were used to establish the mechanism of the formation of CCNPs. By comparing the values of the enthalpy of the mixing of the binary systems, as well as the thermochemical analysis of the reduction, it can be assumed that the first homogeneous formation was due to the entire volume of Pd and Cu, consequently possessing a high negative value of mixing enthalpy with almost all elements. Platinum has a slightly lower negative enthalpy of mixing with almost all elements, and can be assumed to form immediately after Pd and Cu. Since Ag has a slightly lower enthalpy of mixing with all elements other than Ni, it can be assumed that Ag is formed after Pt, and then Ni. All the elements were homogeneously distributed throughout the CCNPs' volume. The formed non-ideal spherical shape of the CCNPs was a consequence of the coagulation of droplets during their transportation to the furnace. Based on the analysed results and literary knowledge, a mechanism for CCNPs' formation was proposed, which is shown in Figure 12.

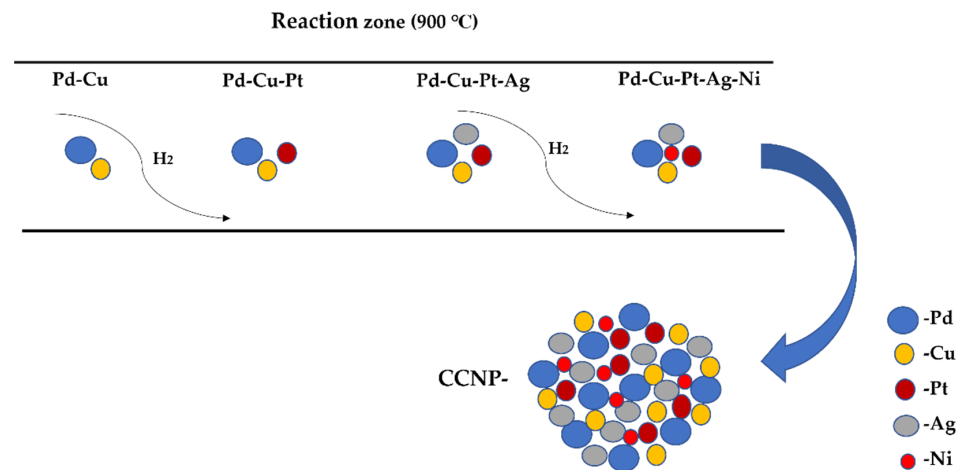


Figure 12. Proposed mechanism for the formation of CCNPs.

5. Conclusions

The following conclusions can be drawn from the present research:

- The hydrometallurgical treatment of the cast $\text{Ag}_{20}\text{Pd}_{20}\text{Pt}_{20}\text{Cu}_{20}\text{Ni}_{20}$ alloy, which involves dissolution with nitric acid, results in an incomplete dissolution of the alloy. As a consequence, a precipitate rich in salts is formed: $(\text{NH}_4)_2\text{PtCl}_6$, $(\text{NH}_3)_6\text{NiPtCl}_6 \times 0.5\text{H}_2\text{O}$, $\text{Pt}_2(\text{NH}_3)_4\text{Cl}_4$. The remaining precursor solution, with a reduced at. % of Pt (11.47) and Ni (3.93), was used for the synthesis of nanoparticles by USP;
- The formatted CCNPs contain a high at. % of Pd, Cu, and Ag and a significantly lower at. % of Pt and Ni compared to the chemical composition of the cast $\text{Ag}_{20}\text{Pd}_{20}\text{Pt}_{20}\text{Cu}_{20}\text{Ni}_{20}$ alloy;
- Lyophilisation has been recognised as a successful method for removing excess water from a suspension with CCNPs avoiding the sedimentation and agglomeration of the nanoparticles;
- The synthesised CCNPs can be classified as medium entropy materials, as indicated by their calculated configurational entropy;
- The mechanism of the formation of CNPs by USP was established so that Pd and Cu are formed first, followed by Pt, while Ag and Ni are formed at the end;
- The presented research showed that it may be possible to use USP and lyophilisation for the synthesis of nanoparticles from waste CCAs. With the help of the hydrometallurgical treatment of CCAs, a precursor solution which enables the synthesis of CCNPs with a bottom-up approach could be prepared. In this way, we can conclude that these two used methods represent technological ways of recycling such materials.

Supplementary Materials: The following supporting information can be downloaded at: <https://www.mdpi.com/article/10.3390/met12111802/s1>.

Author Contributions: Conceptualisation, L.S., S.S., I.A. and R.R.; methodology, L.S., S.S. and R.R.; software, Ž.J. and R.B.; validation, S.S., M.Z., I.A. and R.R.; formal analysis, L.S., S.S., Ž.J. and R.B.; investigation, L.S., S.S. and R.R.; resources, B.F., I.A. and R.R.; data curation, L.S.; writing—original draft preparation, L.S., S.S. and R.R.; writing—review and editing, S.S. and R.R.; supervision, B.F. and R.R.; project administration, B.F.; funding acquisition, S.S., I.A. and R.R. All authors have read and agreed to the published version of the manuscript.

Funding: This research was funded by Javna Agencija za Raziskovalno Dejavnost RS (ARRS), grant number P2-0120, I0-0029, as well as by the DAAD project.

Acknowledgments: The authors greatly acknowledge Peter Majerič, University of Maribor, and the Faculty of Mechanical Engineering for their assistance with the SEM/EDS analyses.

Conflicts of Interest: The authors declare no conflict of interest.

Abbreviations

CCAs	complex concentrated alloys
CCNPs	complex concentrated nanoparticles
DLS	dynamic light scattering
EDS	energy dispersive X-ray spectrometer
HEA	high-entropy alloy
ICP–OES	inductively coupled plasma–optical emission spectrometry
PVP	polyvinylpyrrolidone
SEM	scanning electron microscopy
TEM	transmission electron microscopy
USP	ultrasonic spray pyrolysis
XRF	X-ray fluorescence spectroscopy

References

- Zhang, Y.; Zuo, T.T.; Tang, Z.; Gao, M.C.; Dahmen, K.A.; Liaw, P.K.; Lu, Z.P. Microstructures and properties of high-entropy alloys. *Prog. Mater. Sci.* **2014**, *61*, 1–93. [[CrossRef](#)]
- Raabe, D.; Tasan, C.C.; Springer, H.; Bausch, M. From high-entropy alloys to high-entropy steels. *Steel Res. Int.* **2015**, *86*, 1127–1138. [[CrossRef](#)]
- Miracle, D.B.; Senkov, O.N. A critical review of high entropy alloys and related concepts. *Acta Mater.* **2017**, *122*, 448–511. [[CrossRef](#)]
- Tiyyagura, H.R.; Majerič, P.; Anžel, I.; Rudolf, R. Low-cost synthesis of AuNPs through ultrasonic spray pyrolysis. *Mater. Res. Express* **2020**, *7*, 055017. [[CrossRef](#)]
- Yang, Y.; Song, B.; Ke, X.; Xu, F.; Bozhilov, K.N.; Hu, L.; Shahbazian-Yassar, R.; Zachariah, M.R. Aerosol Synthesis of High Entropy Alloy Nanoparticles. *Langmuir* **2020**, *36*, 1985–1992. [[CrossRef](#)]
- Yeh, J.W. Alloy design strategies and future trends in high-entropy alloys. *JOM* **2013**, *65*, 1759–1771. [[CrossRef](#)]
- Majerič, P.; Rudolf, R. Advances in ultrasonic spray pyrolysis processing of noble metal nanoparticles—Review. *Materials* **2020**, *13*, 3485. [[CrossRef](#)]
- Rahemi Ardekani, S.; Sabour Rouh Aghdam, A.; Nazari, M.; Bayat, A.; Yazdani, E.; Saievar-Iranizad, E. A comprehensive review on ultrasonic spray pyrolysis technique: {Mechanism}, main parameters and applications in condensed matter. *J. Anal. Appl. Pyrolysis* **2019**, *141*, 104631. [[CrossRef](#)]
- Stopić, S.; Dvorak, P.; Friedrich, B. Synthesis of spherical nanosized copper powder by ultrasonic spray pyrolysis. *World Metall. -ERZMETALL* **2005**, *58*, 191–197.
- Stopić, S.; Friedrich, B.; Schroeder, M.; Weirich, T.E. Synthesis of TiO₂ core/RuO₂ shell particles using multistep ultrasonic spray pyrolysis. *Mater. Res. Bull.* **2013**, *48*, 3633–3635. [[CrossRef](#)]
- Gürmen, S.; Stopić, S.; Friedrich, B. Synthesis of nanosized spherical cobalt powder by ultrasonic spray pyrolysis. *Mater. Res. Bull.* **2006**, *41*, 1882–1890. [[CrossRef](#)]
- Kaya, E.E.; Kaya, O.; Stopić, S.; Gürmen, S.; Friedrich, B. Ndfeb magnets recycling process: An alternative method to produce mixed rare earth oxide from scrap ndfeb magnets. *Metals* **2021**, *11*, 716. [[CrossRef](#)]
- Kumar Katiyar, N.; Biswas, K.; Yeh, J.-W.; Sharma, S.; Sekhar Tiwary, C. A perspective on the catalysis using the high entropy alloys. *Nano Energy* **2021**, *88*, 106261. [[CrossRef](#)]
- Xie, P.; Yao, Y.; Huang, Z.; Liu, Z.; Zhang, J.; Li, T.; Wang, G.; Shahbazian-Yassar, R.; Hu, L.; Wang, C. Highly efficient decomposition of ammonia using high-entropy alloy catalysts. *Nat. Commun.* **2019**, *10*, 4011. [[CrossRef](#)]
- Nellaiappan, S.; Katiyar, N.K.; Kumar, R.; Parui, A.; Malviya, K.D.; Pradeep, K.G.; Singh, A.K.; Sharma, S.; Tiwary, C.S.; Biswas, K. High-Entropy Alloys as Catalysts for the CO₂ and CO Reduction Reactions: Experimental Realization. *ACS Catal.* **2020**, *10*, 3658–3663. [[CrossRef](#)]
- Huang, X.; Yang, G.; Li, S.; Wang, H.; Cao, Y.; Peng, F.; Yu, H. Noble-metal-based high-entropy-alloy nanoparticles for electrocatalysis. *J. Energy Chem.* **2022**, *68*, 721–751. [[CrossRef](#)]
- Rudolf, R. Cast Microstructure of a Complex Concentrated Noble Alloy. *Materials* **2022**, *15*, 4788.
- Köroğlu, M.; Ebin, B.; Stopić, S.; Gürmen, S.; Friedrich, B. One step production of silver-copper (AgCu) nanoparticles. *Metals* **2021**, *11*, 1466. [[CrossRef](#)]
- Tang, Z.; Jung, E.; Jang, Y.; Bhang, S.H.; Kim, J.; Kim, W.-S.; Yu, T. Facile Aqueous-Phase Synthesis of Bimetallic. *Materials* **2020**, *13*, 254. [[CrossRef](#)]
- Rudolf, R.; Friedrich, B.; Stopić, S.; Anžel, I.; Tomić, S.; Čolić, M. Cytotoxicity of gold nanoparticles prepared by ultrasonic spray pyrolysis. *J. Biomater. Appl.* **2012**, *26*, 595–612. [[CrossRef](#)]
- Jelen, Ž.; Majerič, P.; Zadravec, M.; Anžel, I.; Rakuša, M.; Rudolf, R. Study of gold nanoparticles' preparation through ultrasonic spray pyrolysis and lyophilisation for possible use as markers in LFIA tests. *Nanotechnol. Rev.* **2021**, *10*, 1978–1992. [[CrossRef](#)]
- Abdelwahed, W.; Degobert, G.; Stainmesse, S.; Fessi, H. Freeze-drying of nanoparticles: Formulation, process and storage considerations. *Adv. Drug Deliv. Rev.* **2006**, *58*, 1688–1713. [[CrossRef](#)] [[PubMed](#)]

23. Psimadas, D.; Georgoulas, P.; Valotassiou, V.; Loudos, G. Molecular Nanomedicine Towards Cancer. *J. Pharm. Sci.* **2012**, *101*, 2271–2280. [[CrossRef](#)]
24. Singh, S.K.; Xu, Q. Bimetallic Ni/Pt nanocatalysts for selective decomposition of hydrazine in aqueous solution to hydrogen at room temperature for chemical hydrogen storage. *Inorg. Chem.* **2010**, *49*, 6148–6152. [[CrossRef](#)] [[PubMed](#)]
25. Mu, X.D.; Evans, D.G.; Kou, Y. A general method for preparation of PVP-stabilized noble metal nanoparticles in room temperature ionic liquids. *Catal. Letters* **2004**, *97*, 151–154. [[CrossRef](#)]
26. Rostek, A.; Breisch, M.; Pappert, K.; Loza, K.; Heggen, M.; Köller, M.; Sengstock, C.; Epple, M. Comparative biological effects of spherical noble metal nanoparticles (Rh, Pd, Ag, Pt, Au) with 4–8 nm diameter. *Beilstein J. Nanotechnol.* **2018**, *9*, 2763–2774. [[CrossRef](#)]
27. Wang, H.; Qiao, X.; Chen, J.; Wang, X.; Ding, S. Mechanisms of PVP in the preparation of silver nanoparticles. *Mater. Chem. Phys.* **2005**, *94*, 449–453. [[CrossRef](#)]
28. Stopić, S.; Ilić, I.; Uskoković, D. Structural and morphological transformations during NiO and Ni particles generation from chloride precursor by ultrasonic spray pyrolysis. *Mater. Lett.* **1995**, *24*, 369–376. [[CrossRef](#)]
29. Švarc, T.; Stopić, S.; Jelen, Ž.; Zadavec, M.; Friedrich, B.; Rudolf, R. Synthesis of Ni/Y₂O₃ Nanocomposite through USP and Lyophilisation for Possible Use as Coating. *Materials* **2022**, *15*, 2856. [[CrossRef](#)]
30. Dauthal, P.; Mukhopadhyay, M. Noble Metal Nanoparticles: Plant-Mediated Synthesis, Mechanistic Aspects of Synthesis, and Applications. *Ind. Eng. Chem. Res.* **2016**, *55*, 9557–9577. [[CrossRef](#)]
31. Shariq, M.; Majerič, P.; Friedrich, B.; Budic, B.; Jenko, D.; Dixit, A.R.; Rudolf, R. Application of Gold(III) Acetate as a New Precursor for the Synthesis of Gold Nanoparticles in PEG Through Ultrasonic Spray Pyrolysis. *J. Clust. Sci.* **2017**, *28*, 1647–1665. [[CrossRef](#)]
32. Ravnik, J.; Ramšak, M.; Zadavec, M.; Kamenik, B.; Hriberšek, M. Experimental and stochastic analysis of lyophilisation. *Eur. J. Pharm. Biopharm.* **2021**, *159*, 108–122. [[CrossRef](#)] [[PubMed](#)]
33. De Temmerman, P.J.; Lammertyn, J.; De Ketelaere, B.; Kestens, V.; Roebben, G.; Verleysen, E.; Mast, J. Measurement uncertainties of size, shape, and surface measurements using transmission electron microscopy of near-monodisperse, near-spherical nanoparticles. *J. Nanoparticle Res.* **2014**, *16*, 2177. [[CrossRef](#)]
34. Horike, C.; Morita, K.; Okabe, T.H. Effective dissolution of platinum by using chloride salts in recovery process. *Metall. Mater. Trans. B: Process Metall. Mater. Process. Sci.* **2012**, *43*, 1300–1307. [[CrossRef](#)]
35. Takeuchi, A.; Inoue, A. Calculation of mixing enthalpy and mismatch entropy. *Mater. T* **2000**, *41*, 1372–1378.
36. Copyright (c) 1996–2021 CrystalMaker Software Limited. Available online: crystallmaker.com (accessed on 20 December 2021).
37. Lin, P.C.; Lin, S.; Wang, P.C.; Sridhar, R. Techniques for physicochemical characterization of nanomaterials. *Biotechnol. Adv.* **2014**, *32*, 711–726. [[CrossRef](#)] [[PubMed](#)]
38. Thompson, J.F.; Miller, E.H. Platinum silver alloys. *J. Am. Chem. Soc.* **1906**, *28*, 1115–1132. [[CrossRef](#)]